JOURNAL OF VIROLOGY, Jan. 2003, p. 1368–1381 Vol. 77, No. 2
0022-538X/03/$08.00+0 DOI: 10.1128/JVI.77.2.1368–1381.2003

Polymorphism and Structural Maturation of Bunyamwera Virus in Golgi and Post-Golgi Compartments

Iñigo J. Salanueva,[1] Reyes R. Novoa,[1] Pilar Cabezas,[1] Carmen López-Iglesias,[2] José L. Carrascosa,[1] Richard M. Elliott,[3] and Cristina Risco[1]*

Department of Macromolecular Structure, Centro Nacional de Biotecnología, CSIC, Cantoblanco, 28049 Madrid,[1] and Universitat de Barcelona, Serveis Cientificotècnics, Unitats de Reconeixement Molecular in situ i Genòmica, 08028 Barcelona,[2] Spain, and Division of Virology, Institute of Biomedical and Life Sciences, University of Glasgow, Glasgow G11 5JR, United Kingdom[3]

Received 14 June 2002/Accepted 10 October 2002

The Golgi apparatus is the assembly site for a number of complex enveloped viruses. Using high-preservation methods for electron microscopy, we have detected two previously unknown maturation steps in the morphogenesis of Bunyamwera virus in BHK-21 cells. The first maturation takes place inside the Golgi stack, where annular immature particles transform into dense, compact structures. Megalomicin, a drug that disrupts the *trans* side of the Golgi complex, reversibly blocks transformation, showing that a functional *trans*-Golgi is needed for maturation. The second structural change seems to take place during the egress of viral particles from cells, when a coat of round-shaped spikes becomes evident. A fourth viral assembly was detected in infected cells: rigid tubular structures assemble in the Golgi region early in infection and frequently connect with mitochondria. In Vero cells, the virus induces an early and spectacular fragmentation of intracellular membranes while productive infection progresses. Assembly occurs in fragmented Golgi stacks and generates tubular structures, as well as the three spherical viral forms. These results, together with our previous studies with nonrelated viruses, show that the Golgi complex contains key factors for the structural transformation of a number of enveloped viruses that assemble intracellularly.

Enveloped viruses are able to use a variety of cellular membranes at different steps of their life cycles. In fact, almost any membranous compartment appears to be used by particular viruses to support their assembly process (27). Viruses that obtain their envelopes intracellularly include flaviviruses (21), herpesviruses (22), hepadnaviruses (13), rubella virus (12), coronaviruses (16), and poxviruses (24). A rather unique morphogenetic pathway has been described for coronaviruses: these assemble large, annular particles by budding into the endoplasmic reticulum-Golgi intermediate compartment (ERGIC). Immature particles later transform into much smaller and denser virions during their transport inside the Golgi stack (29). Key factors located in the *trans*-Golgi subcompartment trigger the spectacular structural transformation of coronaviruses, in which the viral particle volume is reduced to half and the organization of the virus changes completely (33).

As part of our general interest in characterizing how viruses use endomembranes, we have being studying the morphogenetic pathway of bunyaviruses, another group that also uses the Golgi complex for their morphogenesis (11, 25). The family *Bunyaviridae* contains more than 300 named isolates classified into five genera: *Orthobunyavirus*, *Hantavirus*, *Nairovirus*, *Phlebovirus*, and *Tospovirus.* With the exception of hantaviruses, which are transmitted in excretions from persistently infected rodents, these viruses are transmitted by arthropod vectors. The prototype of the family, Bunyamwera virus, is the subject of this report. Several viruses of the family are considered "emerging viruses" that exhibit a worldwide distribution and cause severe disease in humans, including hemorrhagic fevers and encephalitis (e.g., Rift Valley fever, La Crosse, Hantaan, Oropouche, and Crimean-Congo hemorrhagic fever viruses) (9).

The extracellular infectious particles of bunyaviruses have been described as spherical structures of around 100 nm in diameter. These particles form after association of the three internal ribonucleoproteins (negative-sense viral RNA segments bound to the nucleocapsid N protein and the RNA polymerase, termed L protein) with intracellular membranes containing two envelope glycoproteins, G1 and G2 (34). As mentioned above, these interactions take place in Golgi membranes. Bunyamwera virus encodes two additional nonstructural proteins, named NSs and NSm, that are synthesized early in infection. NSs acts as a virulence factor by helping the virus to shut off host cell protein synthesis and to inhibit interferon production (6). In addition, NSs protein controls the activity of the viral polymerase (40). The role of NSm remains to be defined, but the fact that this protein accumulates in the Golgi complex suggests a potential role in virus assembly (26). The reasons for the unusual assembly location in Golgi are not understood, but it is proposed that a Golgi retention signal in one of the viral glycoproteins directs assembly to Golgi membranes (19). Immunocytochemical studies and infections at 15°C showed that Uukuniemi virus, a phlebovirus, assembles both in the pre-Golgi intermediate compartment and in the Golgi stack (14). Some New World hantaviruses are rather different in that assembly occurs in the plasma membrane and spherical particles with rod-like protrusions instead of round-

* Corresponding author. Mailing address: Centro Nacional de Biotecnología, CSIC, Campus Universidad Autónoma, Cantoblanco, 28049 Madrid, Spain. Phone: 34-91-5854550. Fax: 34-91-5854506. E-mail: crisco@cnb.uam.es.

shaped virions are produced (10). Simultaneous assembly in the Golgi complex and plasma membrane has been described as a rare event for Rift Valley fever phlebovirus (1). There is no characterization of the potential cellular factors acting in replication or assembly or of how and where the replication complexes are built.

With the help of cryomicroscopy methods applied to infected cells, we have studied the morphogenesis of Bunyamwera virus in two different cell types and have found a unique assembly pathway and viral polymorphism. Nowadays it is possible to overcome the intrinsic difficulties in correct ultrastructural preservation of large structures such as cells during processing for cryomicroscopy (15). As a direct consequence of these technical advances, we are getting closer to native structures than ever before. In fact, cryomicroscopy represents a revolution in biology (3, 20). The use of high-preservation methods at the ultrastructural level and the study of the dynamic phase of assembly with drugs that block intracellular transport are providing totally new information on how different viruses interact with intracellular membranes to assemble new infectious particles (2, 31, 33). Our present study shows that the Golgi complex, and in particular the *trans* subcompartment, is the central organelle for the first structural maturation of bunyaviruses. As described for the unrelated coronaviruses, a functional *trans*-Golgi is necessary for maturation of viral immature precursors. A second structural transformation takes place during egress of the viral particles to the extracellular environment. In addition, a new virus-related structure of unknown function, but intimately connected with the early phase of infection, is built in the Golgi area. We finally show that the virus causes an early and spectacular fragmentation of endomembranes in Vero cells, in which, however, the virus presents a similar, Golgi-dependent, morphogenetic pathway.

MATERIALS AND METHODS

Cells, virus, and antibodies. BHK-21 (C-13) and Vero cells, supplied by the American Type Culture Collection, were grown in Dulbecco's modified Eagle's medium (DMEM) supplemented with 10% (BHK-21) or 5% (Vero) fetal calf serum (Gibco). Bunyamwera virus (original V-565-001-522), obtained from the American Type Culture Collection, was propagated and subjected to titer determination in BHK-21 cells as described previously (39).

The antiserum against the extracellular form of Bunyamwera virus, the anti-N polyclonal antiserum, and the monoclonal antibody against Bunyamwera G1 protein were described previously (17, 39, 40). The anti-giantin antiserum was kindly provided by M. Renz (Institute of Immunology and and Molecular Genetics, Karlsruhe, Germany), the G1/93 monoclonal antibody, specific for the ERGIC-53 protein, was a kind gift of H. P. Hauri (Biozentrum, University of Basel, Basel, Switzerland), and the anti-PDI antibody was obtained from Affinity Bioreagents, Inc. (Golden, Colo.). The anti-tubulin (T3526) and anti-vimentin (V9 monoclonal antibody) were obtained from Sigma. Secondary antibodies conjugated with rhodamine or fluorescein were supplied by Southern Biotechnology Associates, Inc. (Birmingham, Ala.). The lectin wheat germ agglutinin (WGA) conjugated with rhodamine was a product of Molecular Probes (Eugene, Oreg.). Phalloidin conjugated with rhodamine was a product of Sigma. Secondary antibodies conjugated with colloidal gold were supplied by BioCell International (Cardiff, United Kingdom).

Infections and treatments with drugs. Multiple-step growth curves of Bunyamwera virus were obtained with BHK-21 and Vero cells. Confluent monolayers were infected with Bunyamwera virus at a multiplicity of infection of 0.001 PFU per cell. The inoculum was removed after a 1-h incubation, and the cells were washed twice with DMEM and overlaid with fresh DMEM supplemented with 2% fetal calf serum. Cells were maintained at 32°C, and supernatants were collected at different times postinfection (p.i.). Virus yields (PFU per milliliter) were determined by titer determination on cell monolayers. For the studies of viral assembly, cell monolayers were infected at 37°C and 1 PFU/ml. At different times p.i., cells were processed for immunofluorescence or fixed for electron microscopy analysis. Some cultures were subjected to treatments with different drugs. Megalomicin (MGM), a Golgi-disrupting drug (5) kindly supplied by B. Alarcón (Centro de Biología Molecular "Severo Ochoa", Madrid, Spain), was added to noninfected or infected cell cultures at a final concentration of 25 or 50 μM and different times p.i. (1, 2, 3, and 4 h p.i.). For Bunyamwera-infected monolayers, MGM was added at 4 h p.i, the option that provided a reversible blockade. The treatment was maintained for 6 h. After removing MGM, some cultures were incubated for 2 h longer in either the presence or the absence of 100 μg of cycloheximide per ml. Supernatants of the cultures were then collected for virus titer determination, and cell monolayers were fixed and processed for immunofluorescence or transmission electron microscopy (TEM).

Fluorescence microscopy. Cell monolayers grown on coverslips were washed with phosphate-buffered saline (PBS) and subjected to different conditions of permeabilization, depending on the specific element to be detected. To detect the Bunyamwera virus N protein, tubulin, or vimentin, cells were permeabilized for 10 min with methanol at −20°C. A mixture of methanol: acetone (1:1) was used to permeabilize cells before incubation with the monoclonal antibody against Bunyamwera G1 glycoprotein or WGA conjugated with rhodamine. For localizing the Golgi protein giantin, the ERGIC-53 protein, or the endoplasmic reticulum marker protein disulfide isomerase, cells were treated with 3% paraformaldehyde for 20 min after being incubated with PBS containing 0.1% bovine serum albumin (BSA). Samples were then incubated with PBS containing 100 mM glycine and permeabilized with methanol (3 min at −20°C). Finally, for actin detection, cells were treated with 4% paraformaldehyde for 15 min, incubated with PBS containing 100 mM glycine, and permeabilized with 0.2% Triton X-100 for 10 min before incubation of the monolayers with 1 μM phalloidin-rhodamine. Dilutions (in PBS containing 0.1% BSA) for the different primary antibodies were as follows: 1:200 for anti-G1, anti-N, and anti-Bunyamwera virus; 1:50 for anti-giantin, anti-ERGIC-53, and anti-PDI; and 1:100 for anti-tubulin and anti-vimentin. After permeabilization and treatment with PBS containing 2% BSA, coverslips were incubated with the corresponding secondary antibodies diluted 1:600 in PBS containing 0.1% BSA, washed with the same buffer, and mounted on glass slides with Mowiol (Aldrich Chemical Co., Milwaukee, Wis.). Samples were studied under a Zeiss Axiophot fluorescence microscope, and images were collected with a MicroMax digital camera system.

EM of cell cultures. (i) Thin-section analysis. Ultrastructural analysis of control and Bunyamwera virus-infected cells was done by conventional embedding or by freeze-substitution and embedding in epoxy-resin EML-812, using procedures previously described in detail (29, 31, 33). Conventional embedding in EML-812 (Taab Laboratories, Adermaston, Berkshire, United Kingdom) was done after chemical fixation in situ in a mixture of 2% glutaraldehyde and 1% tannic acid in HEPES buffer, followed by a short dehydration series at 4°C. Freeze-substitution was performed in a dedicated automated freeze substitution unit (AFS; Leica-Reichert-Jung, Vienna, Austria) on cells previously frozen in liquid propane and subsequently substituted at −90°C in pure acetone containing 1% osmium tetroxide. Ultrathin sections approximately uniform in width (30 to 40 nm) were either stained with uranyl acetate and lead citrate or subjected to detection of specific components.

(ii) Ultrastructural labeling of specific components. Bunyamwera virus proteins were detected on thin sections of freeze-substituted samples or on frozen-hydrated cryosections. Immunolabeling on conventional thin sections was performed by well-established procedures, previously described in detail (28, 31). For ultrastructural detection of RNA, a complex of RNase and 10-nm-diameter colloidal gold (EY Laboratories, San Diego, Calif.) was used as described previously (29). Thin-sections from freeze-substituted samples were collected on gold electron microscopy (EM) grids covered with Formvar and carbon and incubated for 30 min at room temperature with the gold conjugate diluted 1:40 in PBS. After being washed with PBS and distilled water, samples were stained with uranyl acetate and lead citrate. To unmask viral RNA molecules, some sections were subjected to the following treatment before incubation with RNase-gold: 15-min incubation at 37°C with proteinase K (1 μg/ml in Tris-EDTA), washing with PBS, 10-min fixation with 4% paraformaldehyde in PBS, washing again with PBS, and incubation for 10 min with 0.2 M NH_4Cl. As a cytochemical control, some sections were preincubated for 30 min at 37°C with a solution of nonconjugated RNase (20 μg/ml) before being treated with the RNase-gold conjugate.

For labeling on cryosections, cell monolayers were chemically fixed at 4°C with a mixture of 4% paraformaldehyde and 0.1% glutaraldehyde in PBS. After being washed with PBS containing 50 mM glycine, the cells were embedded in gelatin, fixed again with 4% paraformaldehyde in PBS, infused gradually from 0.6 to 2.3

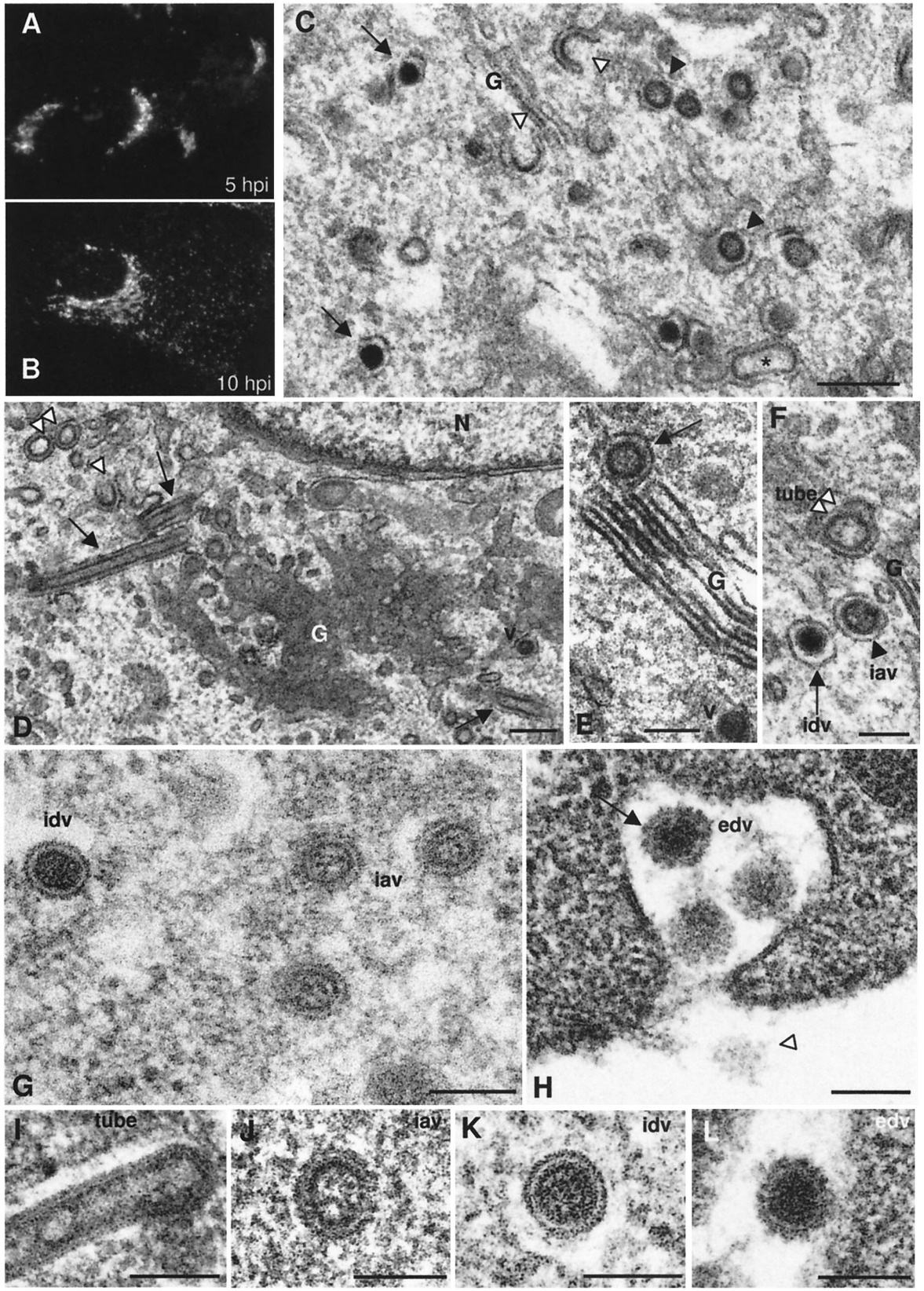

FIG. 1. Progression of infection by Bunyamwera virus in BHK-21 cells. (A and B) Immunofluorescence detection of G1 protein at 5 h p.i. (A) and 10 h p.i. (B). (C) EM of the Golgi area in a BHK-21 cell at 10 h p.i. (conventional processing). At least four potential types of virus-related structures are distinguished: budding arcs (white arrowheads), annular spherical particles (black arrowheads), dense spherical particles (arrows), and elongated tube-like structures (asterisk). (D) Typical view of perinuclear Golgi membranes with tubular structures: arrows point to longitudinal

M sucrose in PBS at 4°C, frozen in liquid propane, and stored in liquid nitrogen. Thin-sections were prepared in an ultracryomicrotome (Leica EM FCS, Vienna, Austria) operating at −120°C. Immunogold labeling was later performed as described previously (37).

(iii) Freeze-fracture. Conventional freeze-fracture was performed as described previously (30, 31). Cell monolayers were chemically fixed in situ, cryoprotected with glycerol, frozen in liquid ethane, and transferred to the BAF 060 freeze-etching unit (Bal-Tec). Fracture was done at −150°C. Metal replicas were done immediately after fracturing by evaporating 2 nm of platinum with an electron gun at an angle of 45° and 20 nm of carbon with an electron gun at an angle of 90°. Replicas were floated in commercial bleach and incubated overnight. After extensive washing in water, the replicas were picked up in Formvar-coated EM grids and studied by EM.

(iv) Processing of viral particles from culture supernatants. Virions released by infected cultures were processed by negative staining, particle counting, or freeze-etching, before being studied by TEM. Negative staining with uranyl acetate and sodium phosphotungstate was performed after adsorbing the viral particles on EM grids made hydrophilic by glow discharge, by using standard procedures (28). The number of particles in cell supernatants was calculated after making a series of dilutions of the virus stocks and a standard solution of latex spheres. This standard, provided by Ted Pella, Inc. (Redding, Calif.), contained latex spheres of 93 nm in diameter and known concentration (2.415×10^{11} particles/ml). After negative staining, samples were studied by TEM and counting was done in the samples containing similar numbers of viral particles and latex spheres.

(v) Imaging and quantitative analysis. Collection of images, measurements, and quantifications were done in a JEOL 1200-EX II electron microscope operating at 100 kV. Electron micrographs were scanned using an Epson Perfection 2450 PHOTO scanner and Picture Publisher 8 software.

RESULTS

Polymorphism of viral assemblies in Bunyamwera virus-infected BHK-21 cells. Bunyaviruses are enveloped viruses that assemble in association with the Golgi complex. This is shown by the typical Golgi staining pattern obtained when localizing the viral glycoprotein G1 by immunofluorescence in Bunyamwera virus-infected BHK-21 cells at early times p.i. (Fig. 1A). A punctate pattern, which corresponds to secretory vesicles filled with viruses, in addition to Golgi labeling was observed at later times p.i. (Fig. 1B). When the ultrastructure of infected cells was studied, different types of potential viral structures were observed in the Golgi area: typical budding profiles or maturation arcs are seen in Golgi membranes, together with annular, round assemblies of intermediate electron density, and electron-dense, compact round particles (Fig. 1C). Annular, larger round assemblies of low electron density were also seen (Fig. 1D). While the two smaller spherical forms are compatible with the size of the virus in thin sections, this is not the case for the larger round structures, which in fact correspond to cross-sectioned tubular assemblies, usually seen on the periphery of Golgi stacks (Fig. 1D) and sometimes clearly seen inside Golgi sacculi (Fig. 1E). The three types of round viral structures are seen on both the *cis* and *trans* sides of the Golgi stacks. They are shown together in Fig. 1F; the smaller structures (intracellular annular viruses [iavs] and intracellular dense viruses [idvs]) have a mean diameter of 61.9 ± 3.8 nm, while the larger structures have a diameter of 95.3 ± 3.4 nm. Since such a viral polymorphism has not been previously described in bunyavirus-infected cells, we then applied freeze-substitution, a method that provides superior preservation of cellular and viral structures (15). The shape and dimensions of the different Bunyamwera virus-related structures were closer to "native" assemblies after freeze-substitution (Fig. 1G to L). The two types of intracellular viral particles detected in the Golgi region have a mean diameter of 82.45 ± 3.9 nm and very different internal structures (Fig. 1G). The less dense forms (or iavs) have a peripheral dense ring and a less dense core that contains some material of undefined structure. The dense form (or idvs) has an apparently smooth external surface with a clear peripheral white halo surrounded by a dark line. The extracellular virus presents a single morphology (Fig. 1H). Virions (extracellular dense viruses [edvs]) are homogeneously dense, but two main features differentiate them from the idvs; the peripheral white halo is less neat, and a prominent coat is present on the surface of the particles (Fig. 1H). As seen in sections through the surface of virions, this coat is composed of round spikes (Fig. 1H). Figures 1I to L show individual representative examples of the four viral structures detected in infected BHK-21 cells. Tubes are filled with material when adequately preserved by freeze-substitution (Fig. 1I). This dense material connects the opposite walls in some regions of the tube. The three spherical viral particles have a similar size but are clearly different in internal and surface organization when visualized in highly preserved samples (Fig. 1J to 1L).

Due to the variety of structures that were detected in Bunyamwera virus-infected cells and were most probably related to the virus, since they are absent in noninfected cells, a detailed analysis of their significance was necessary. First, their viral nature was confirmed by immunogold detection of Bunyamwera virus proteins on sections of freeze-substituted samples (where the described viral morphologies are well defined) by using an anti-Bunyamwera virus polyclonal antiserum raised against the extracellular viral form. This antiserum provided weak to moderate signals on all viral forms described above (Fig. 2A to C). Labeling on cryosections, where the different viral morphologies are difficult to distinguish, rendered stronger labeling signals that confirmed the viral nature of the tubular structures (Fig. 2D). When an RNase-gold complex was used, similar signals were obtained for all viral forms and for viral tubes (Fig. 2E to H). Positive RNA-associated control signals were obtained in the ribosomes of the rough endoplasmic reticulum (RER) (Fig. 2I), while the RNase-treated negative controls lacked any labeling either on ribosomes or on viral particles (Fig. 2J). Thus, from the experiments with specific antibodies, the tubes and the three types of spherical

sections of tubes, while the double white arrowhead points to cross-sectioned tubes. The single white arrowhead points to a budding arc, while a viral particle is marked with v. (E) Some tubes are seen inside Golgi sacculi (arrow). (F) The three types of round viral assemblies detected in Golgi stacks are shown together: the double white arrowhead points to the cross-section of a tube, the black arrowhead points to an IAV, and the arrow points to an IDV. (G to L) Freeze-substituted infected cells showing the structure and dimensions of the different viral assemblies after high-preservation processing methods. (G) Three annular, less dense particles (IDVs) are seen on the right, while a dense virus (IDV) is seen on the left. (H) EDVs contain a dense surface layer of spikes (arrow) absent in IDVs. The white arrowhead in panel H points to a surface section of an extracellular particle, where the arrangement of surface spikes can be seen. (I) tube; (J) IAV; (K) IDV; (L) EDV. Bars: 200 nm (C and D); 100 nm (E to L).

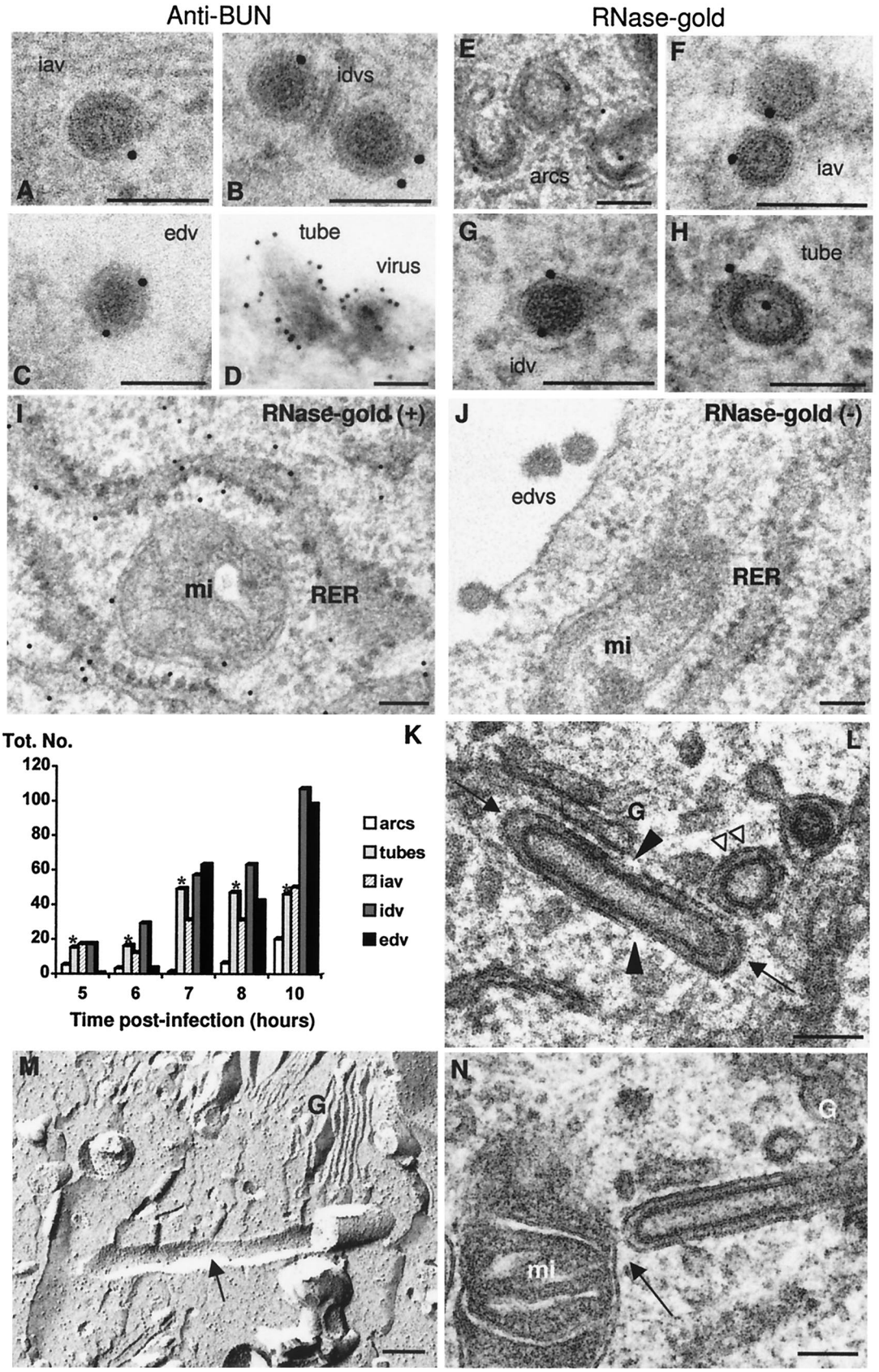
Anti-BUN
RNase-gold
iav
idvs
A
B
E
arcs
F
iav
edv
tube
virus
C
D
G
idv
H
tube
I
RNase-gold (+)
mi
RER
J
RNase-gold (-)
edvs
RER
mi
Tot. No.
120
100
80
60
40
20
0
5
6
7
8
10
Time post-infection (hours)
K
arcs
tubes
iav
idv
edv
L
G
M
G
N
G
mi

particles are all related to Bunyamwera virus and also contain RNA. In Fig. 2K, quantification of viral assemblies at different times p.i. is shown. The numbers of extracellular viruses were underestimated since we can quantify only the viral particles adsorbed on the cell surface. We observed that tubes and iavs were early assemblies, restricted to the Golgi apparatus, while idvs were located both in the Golgi complex and inside secretory vesicles. The fact that these two viral forms coexisted in the Golgi complex strongly suggests that there is a first structural maturation that occurs in this compartment of the secretory pathway. Tubes were formed from the beginning of infection, being detected at the same time as the first viral particles (at 5 h p.i.). The tubes increased in numbers from 6 to 7 h p.i., their numbers stabilized from 7 to 10 h p.i., and then their relative amounts declined at later times, such as 24 and 48 h p.i. (data not shown). With the use of serial sections, we could usually detect several tubes (often one to three tubes) per Golgi stack (data not shown). Thus, while both idvs and edvs increase in number with time, the early formation of tubes and the stabilization of their numbers suggest that they might play a role before the assembly of mature viruses. These very unusual tubular structures were detected only in the Golgi region, sometimes inside the Golgi sacculi and frequently on the periphery of the stacks. They frequently exhibited closed ends, a variety of orientations, and open areas (Fig. 2L). The length of the tubes with both ends closed was variable, from 200 nm to more than 1 μm. In addition, their structure seemed to be rather rigid, as suggested by freeze-fracture (Fig. 2M). Physical contacts between viral particles and tubes were not detected. Another outstanding feature of these tubes was that they projected out of the Golgi and their membranes frequently connected with the external membrane of surrounding mitochondria (Fig. 2N).

Effects of Golgi-disrupting drugs on Bunyamwera virus assembly and maturation. The use of drugs that block transport along the secretory pathway has proven very useful in studying intracellular transport and subsequently in dissecting the morphogenesis of viruses that assemble in particular intracellular membranes. We used MGM in an attempt to understand the Golgi-associated maturation of Bunyamwera virus (Fig. 3). MGM is a macrolide antibiotic that reversibly alters the *trans* side of the Golgi complex in different cell types, causing minor alterations in the *cis* and medial subcompartments (5). The reversible effect of MGM on the *trans*-Golgi in both control and infected BHK-21 cells, here detected with WGA, is shown in Fig. 3A to C. The swelling and spreading of this Golgi subcompartment reverted 2 h after removal of the drug from the cultures, and reversion was more homogeneous within the monolayer when the drug was added at 25 μM than at 50 μM. The lower concentration of the drug was chosen for the following experiments. In Bunyamwera virus-infected cells, the *trans* side of the Golgi was also reversibly disrupted by MGM (Fig. 3D to F). At the ultrastructural level, this swelling of the *trans*-Golgi was seen as large vacuoles filled with small vesicles and dense material still in contact with Golgi sacculi (Fig. 3G). MGM did not significantly affect the *cis*-Golgi of BHK-21 cells, as observed with an anti-giantin antibody (Figs. 3H and I). When MGM was added to Bunyamwera virus-infected cultures at 4 h p.i., the virus (as detected with the anti-G1 antibody) stayed close to the cell nucleus in a *cis*-Golgi-like location (Fig. 3J). When the drug was removed from cultures after 6 h of treatment, the virus-associated signal reverted 2 h later to the punctate pattern characteristic of secretory vesicles filled with viruses (Fig. 3K). At the ultrastructural level, the disrupted Golgi stacks in infected MGM-treated cells had arcs, tubes, and immature viruses almost exclusively (Fig. 3L). Nondisrupted stacks, very similar to Golgi complexes from infected untreated cells, were also occasionally observed (data not shown). When MGM was removed from the cultures, dense mature viruses formed again in partially recovered Golgi stacks (Fig. 3M). When reversion of MGM was done in the presence of the protein synthesis inhibitor cycloheximide, thereby preventing the formation of new virions, we could monitor the evolution of the previously accumulated structures. Under these conditions, the number of intracellular viral structures decreased considerably while the presence of virions in the extracellular environment was restored (Fig. 3N). Quantitative analysis of the different conditions described is summarized in Fig. 3O. Maturation arcs, tubes, and iavs accumulated with MGM treatment. Their numbers decreased after reversion of the drug's effects, while the numbers of idvs and edvs increased. These data demonstrate that the, less dense annular viral structures are the immature precursors of the dense mature virions, that transformation takes place in the Golgi stack, and that a functional *trans*-Golgi is necessary for this maturation to proceed normally.

Second maturation step for Bunyamwera virus. As shown in Fig. 1, Bunyamwera virus edvs are morphologically distinct from the idvs. This raised the question of the location of the second maturation step: do the particles find a factor that triggers the second transformation as they exit the Golgi complex, during their transport from the Golgi to the cell surface, or at the moment of secretion? To address this question, we carefully studied the morphology of the viral particles seen in post-Golgi locations. However, the contour of the particles was frequently masked by material inside secretory vesicles, mak-

FIG. 2. Cytochemical characterization and quantification of the different virus-related assemblies in BHK-21 cells (A to H). An anti-Bunyamwera virus antiserum (A to D) and a complex of RNase and colloidal gold (E to H) were used. A cryosection is shown in panel D, while sections of freeze-substituted samples are shown in panels A to C and E to J. The specificity of RNase-gold labeling was assessed with positive (I) and negative (J) controls. (K) Distribution of the different viral assemblies in BHK-21 cells at early times p.i. For quantification, 25 infected cells were studied at 6, 7, 8, 10, 24, and 48 h p.i. On the other hand, 50 cells were studied at 5 h p.i. The total number of structures is indicated on the *y* axis for each time p.i. A total of 1,194 viral structures were included in the quantification. Bars representing the number of viral tubes are marked with asterisks. (L) These tubes were frequently observed as structures with both ends closed (arrows), interrupted membranes (black arrowheads), and different arrangements within the Golgi stack (arrows and double white arrowhead). (M) Tube (arrow) associated to the Golgi stack (G), as visualized by freeze-fracture. (N) Golgi-associated tubes and mitochondria were frequently connected (arrow). G, Golgi complex; mi: mitochondria. Bars, 100 nm.

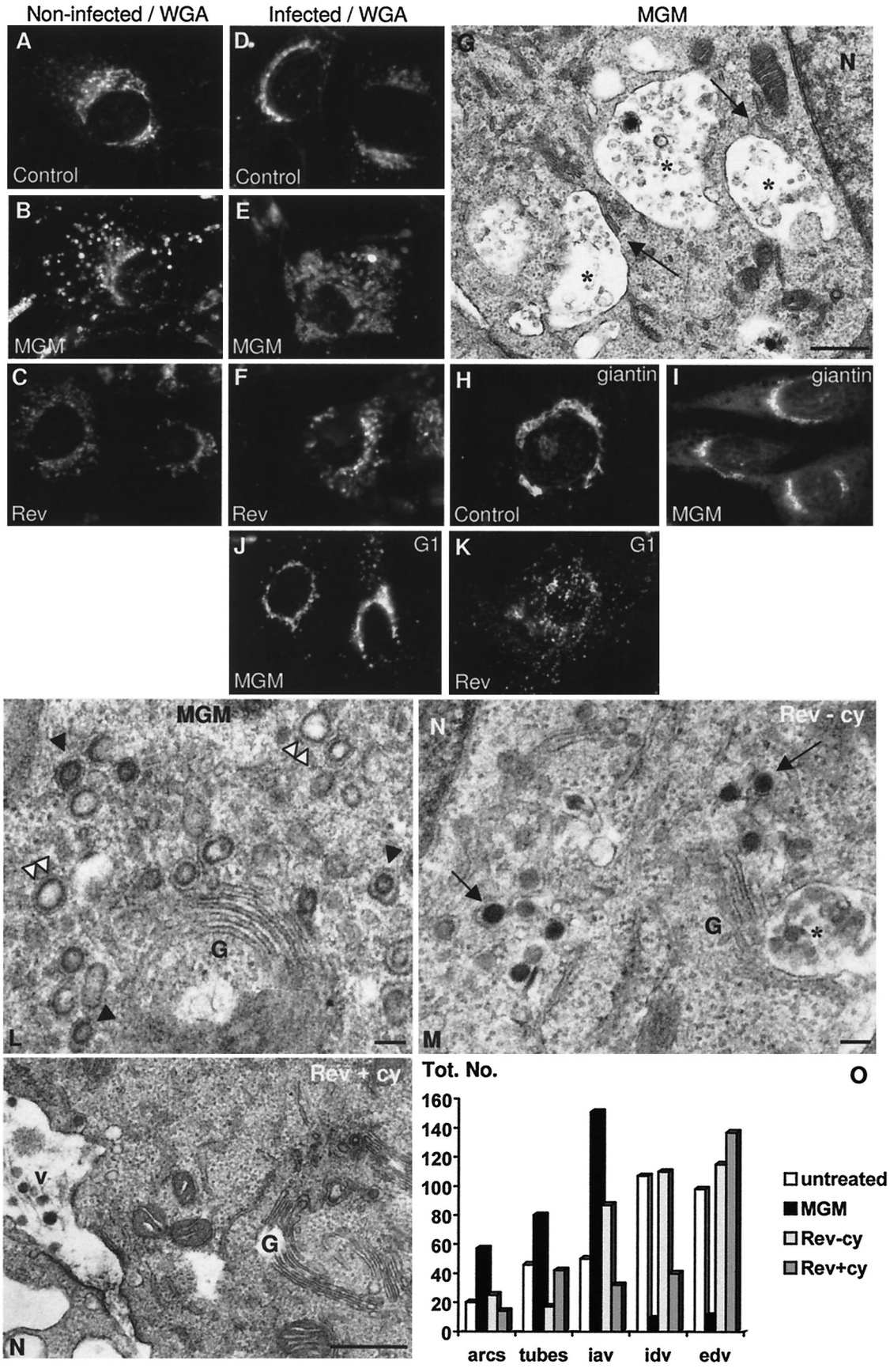
Non-infected / WGA
Infected / WGA
MGM
A
Control
D
Control
G
N
B
MGM
E
MGM
C
Rev
F
Rev
H
giantin
Control
I
giantin
MGM
J
G1
MGM
K
G1
Rev
MGM
G
L
N
Rev - cy
G
M
Rev + cy
v
G
N
Tot. No.
O
160
140
120
100
80
60
40
20
0
arcs
tubes
iav
idv
edv
untreated
MGM
Rev-cy
Rev+cy

ing analysis difficult in most cases. We then attempted to trace viral particles by immunogold labeling on cryosections. Viral particles showed variable reactivity depending on their location (Fig. 4). Particles within the Golgi complex exhibited a moderate signal when a polyclonal antisera raised against the extracellular virion was used (Fig. 4A), and weak labeling was detected for the viral particles inside secretory vesicles, as shown in Fig. 4A and B. In Fig. 4B it can be observed that viruses inside secretory vesicles that reached the plasma membrane were weakly labeled while viruses already on the cell surface reacted strongly. The final conformation of the viral glycoproteins that generates the compact, dense layer of surface spikes (clearly visible on thin sections of freeze-substituted viruses, as shown in Fig. 1H and L) seems to be acquired when the virus exits the cell. At this location, the mature viruses become fully recognizable by the anti- virion antibodies (Fig. 4C and D). Surface spikes in fully mature viruses were visualized by negative staining of isolated particles and exhibited a rough surface with uranyl acetate (Fig. 4E), but a well-defined layer of round structures was distinguished with sodium phosphotungstate (Fig. 4F).

Morphogenetic pathway of Bunyamwera virus in Vero cells. After discovering the unexpectedly complex morphogenesis of Bunyamwera virus in BHK-21 cells, with at least two structural maturation steps associated with transport of viral particles along the secretory pathway, we analyzed viral assembly in Vero cells. With immunofluorescence staining to monitor the progression of Bunyamwera virus infection in Vero cells, a very different infection pattern was obtained (Fig. 5). No characteristic Golgi-associated signal was distinguished; instead, a punctate staining pattern was observed at all times during infection (Fig. 5A and B) while no characteristic Golgi pattern (Fig. 5C) was ever obtained when labeling for viral antigen. This suggested that there were fundamental differences in the assembly pathway of the virus in the two cell types and that morphogenesis could be Golgi independent in Vero cells. However, when staining for the Golgi complex in infected Vero cells, a spectacular fragmentation and dispersion of Golgi membranes was observed (Fig. 5D and E). This early disruption was completed before G1 viral glycoprotein could be detected by immunofluorescence, and viral particles are seen by EM (see below). In fact, approximately 50% of cells in the monolayers had fully fragmented Golgi complexes by 3 h p.i., coincident with a similar percentage of cells showing cytoplasmic accumulation of the viral N protein (data not shown). All cells in the monolayers were affected at 5 h p.i. Other intracellular membranous entities of the secretory pathway were also disrupted at an early phase of Bunyamwera virus infection: the ERGIC was so fragmented that the signal for this compartment almost disappeared (Fig. 5F to H). The RER was also affected, with an apparent collapse in some areas (Fig. 5I and J). In contrast, no major alterations to these three membranous compartments in infected BHK-21 cells were detected (data not shown). Double immunofluorescence labeling at different times p.i. showed that G1 actually accumulated in Golgi fragments in Vero cells. Colocalization of the viral protein G1 and the *cis*-Golgi marker giantin was detected during the early phase of infection (Fig. 5K and L). Colocalization of G1 with the *trans*-Golgi marker WGA was also detected (data not shown). Taking into account the general effects on endomembranes, we considered the possibility that alterations in the cytoskeleton could be responsible. However, immunofluorescence localization of actin, vimentin, and tubulin (Fig. 5M and N) showed that only the microtubular network suffered some alterations during infection. At 5 h p.i., 2 h after the general disruption of endomembranes, peripheral bundling of microtubules and some disorganization of the network was observed (Fig. 5M and N).

Ultrastructural analysis of Bunyamwera virus-infected Vero cells confirmed that the virus caused microvesiculation and disassembly of endomembranes (Fig. 6). Compared to control cells (Fig. 6A), infected cells showed a less dense cytoplasm, dense mitochondria, and fragmented Golgi and RER cisternae (Fig. 6B and C). At early times p.i. (6 to 8 h p.i.), sacculi within fragmented Golgi stacks were still visible (Fig. 6B), but at later times (more than 10 h p.i.), the morphology of most of the stacks was lost (data not shown). Although the effects on cellular ultrastructure were marked, no evidence for cell lysis was detected between 4 and 16 h p.i. Accumulation of viral proteins in the fragments of Golgi stacks was followed by the formation of tubes and viral particles: freeze-substitution showed viral assemblies indistinguishable from the viral forms described in BHK-21 cells, including Golgi-associated tubes, iavs, and idvs (Fig. 6D to G). Tubes in the Golgi region had some areas open to the cytoplasm (Fig. 6D) and were frequently seen in contact with mitochondria (Fig. 6E). Extracellular virions also contained the prominent layer of spikes (Fig. 6H). These observations suggest that fragmented Golgi stacks are able to sup-

FIG. 3. MGM treatment of BHK-21 cells. (A and B) Immunofluorescence localization of the *trans* side of the Golgi complex (with the lectin WGA) in noninfected untreated (A), and MGM-treated (B) BHK-21 cells. (C) Reversal of the drug's effects. (D to F) WGA labeling shows similar MGM effects on Bunyamwera virus-infected BHK-21 cells. (D) Cells at 10 h p.i. (E) Cell at 10 h p.i. but with the last 6 hours in the presence of MGM; (F) Cell subjected to the same treatment as in panel E but incubated for 2 h after removing the drug. (G) Ultrastructure of BHK-21 cells after MGM treatment. Asterisks mark the swollen *trans*-Golgi subcompartments, some of them still attached to the Golgi sacculi. (H and I) Localization of the *cis* side of the Golgi complex (with an anti-giantin antiserum) in noninfected untreated (H) and MGM-treated (I) cells. (J and K) Localization of Bunyamwera virus G1 protein during MGM treatment in infected cells (J) and after reversal of the drug's effects (K). (L) Accumulation of tubes (double white arrowheads) and annular viruses (black arrowheads) in Golgi membranes of MGM-treated cells. (M) Accumulation of dense intracellular viruses (arrows) in Golgi membranes after reversal of the effects of MGM in the absence of cycloheximide. (N) After reversal of the effects of MGM in the presence of cycloheximide, the number of intracellular viruses decreases and the edvs (v) are more abundant. (O) Quantification of the different viral assemblies in untreated infected cells and in infected cells subjected to the different treatments: "untreated" cells are BHK-21 cultures at 10 h p.i. without MGM treatment; "MGM" cells at 4 h p.i. were treated with the drug until 10 h p.i.; "Rev-cy" corresponds to cells treated with the drug as in "MGM" and incubated for a further 2 h after removing the drug from the cultures (total, 12 h p.i.); finally, "Rev+cy" corresponds to cells also subjected to 2 h of reversion of the effects of MGM but in the presence of 100 μg of cycloheximide per ml. A total of 1,254 viral structures were included in the quantification. N, nucleus. Bars, 0.5 μm (G and N); 100 nm (L and M).

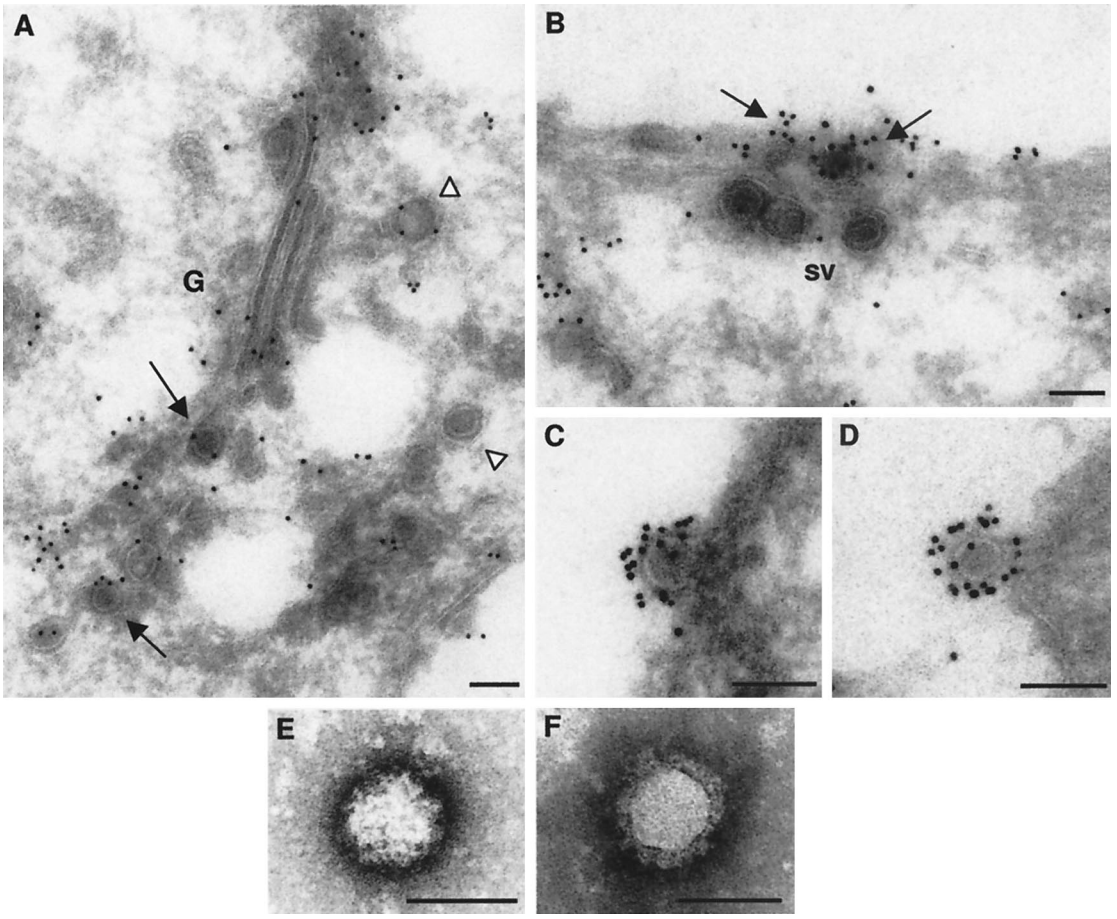

FIG. 4. Second maturation step for Bunyamwera virus in BHK-21 cells. (A to D) Labeling with anti-Bunyamwera virus antiserum on cryosections of infected cells. (A) Viral particles inside the Golgi complex (G) are marked with arrows (moderate labeling), while viruses in the post-Golgi area are marked with arrowheads (weak to moderate labeling). (B) Viral particles inside secretory vesicles (sv) reaching the plasma membrane exhibiting weak labeling. They are near an area where viral particles are already exiting the cell and are strongly labeled (arrows). (C and D) Extracellular viral particles attached to the cell surface, exhibiting strong labeling on their periphery. (E and F) Extracellular viral particles visualized after negative staining with uranyl acetate (E) and sodium phosphotungstate (F). The surface spikes are clearly distinguished in the latter. Bars, 100 nm.

port the structural maturation of Bunyamwera virus, since iavs and idvs coexisted in the remnants of this compartment. Quantitative analysis of the different viral assemblies early in infection showed a process comparable to that described for BHK-21 cells, although with a lower accumulation of intracellular viruses in Vero cells (Fig. 6I). It seems, therefore, that assembly in Vero cells is rapidly followed by transport to the cell surface and release from the cell. Multiple-step growth curves showed that Bunyamwera virus production in this cell type reached 4×10^6 to 1×10^7 PFU/ml at 72 h p.i., following infection at 32°C and at a MOI of 0.001 PFU/ml (Fig. 6J). Under the same conditions, titers from infected BHK-21 cells reached 1×10^7 to 1×10^8 PFU/ml. The virus formed smaller plaques in monolayers of Vero cells than of BHK-21 cells (insets in Fig. 6J). The ratio of infectious particles to physical particles was also similar for the virus released by the two cell lines: 1 to 30 for BHK-21 cells, and 1 to 40 for Vero cells. Thus, despite the generalized disruption of endomembranes in Vero cells, Bunyamwera virus establishes a productive infection and uses the morphologically altered Golgi stacks for assembly and maturation.

DISCUSSION

With the key contribution of high-preservation methods at the EM level, we have been studying how complex viruses use intracellular membranes for their assembly. We previously reported that coronaviruses transform inside the Golgi stack when immature particles reach the *trans* subcompartment, through a novel maturation process (29, 33). Here we show that bunyaviruses also depend on a functional *trans*-Golgi for structural transformation, pointing to a more general mechanism that previously expected. The pathway, however, is more complex for bunyaviruses.

Assembly of Bunyamwera virus in BHK-21 cells. As summarized in Fig. 7, a large structure is formed in the perinuclear area of infected cells. Golgi stacks in contact with mitochondria build a "viral factory" for Bunyamwera virus. Viral assem-

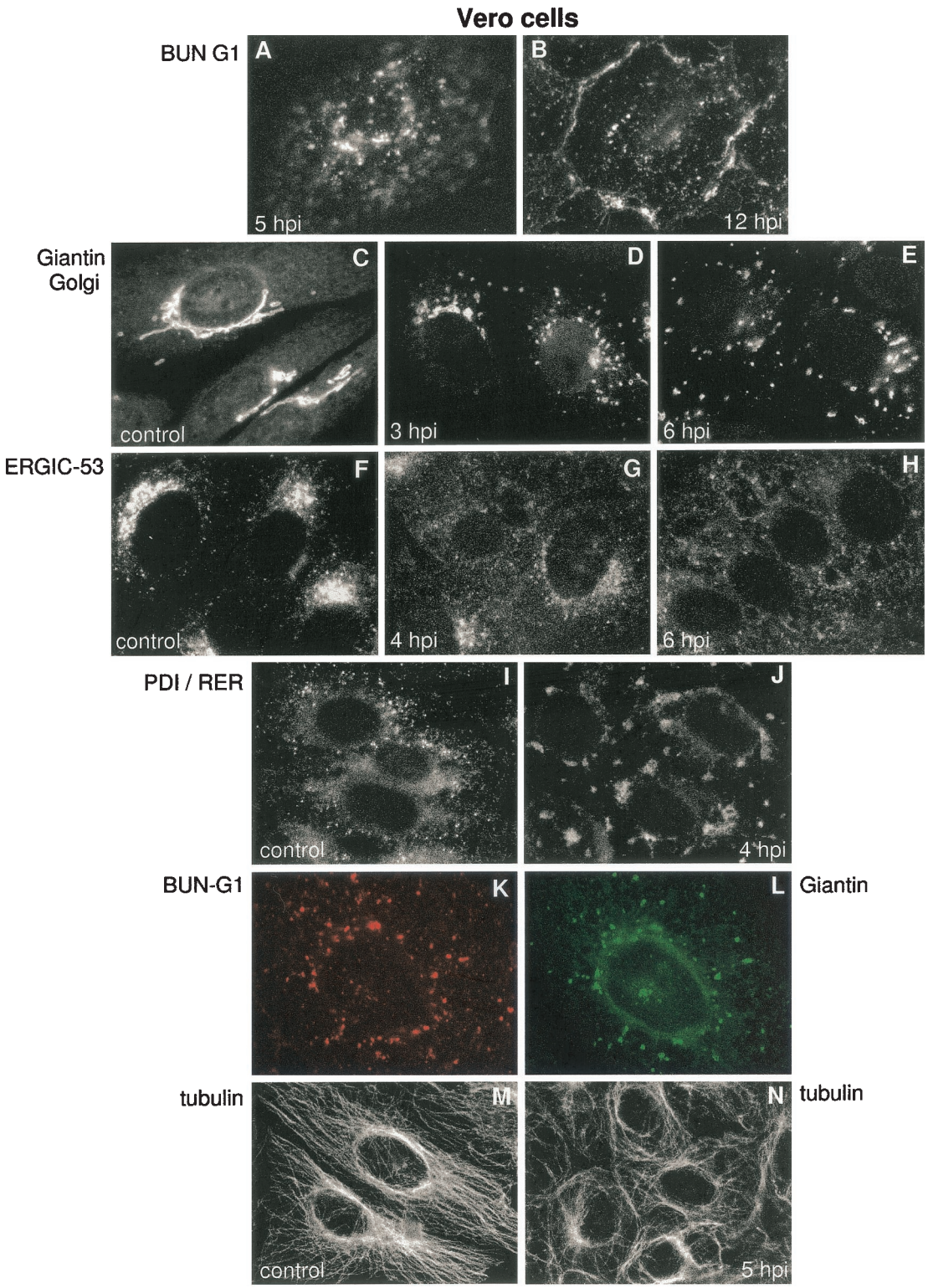

FIG. 5. Progression of Bunyamwera virus infection in Vero cells. (A and B) Immunofluorescence localization of Bunyamwera virus G1 protein at 5 h p.i. (A) and 12 h p.i. (B). (C to E) Immunofluorescence detection of Golgi with an anti-giantin antiserum in noninfected cells (C) and in infected cells at 3 h p.i. (D) and 6 h p.i. (E). (F to H) Detection of ERGIC with an anti-ERGIC-53 monoclonal antibody in noninfected cells (F) and in cells infected at 4 h p.i. (G) and 6 h p.i. (H). (I and J) Detection of the RER with an anti-protein disulfide isomerase (PDI) antiserum, both in noninfected cells (I) and in Bunyamwera virus-infected cells at 4 h p.i. (J). (K and L) Double-immunofluorescence localization of Bunyamwera virus G1 (K) and Golgi membranes (L) at 6 h p.i. (M and N) The organization of the microtubular network is shown in noninfected (M) and infected (N) cells at 5 h p.i., using an anti-tubulin antibody.

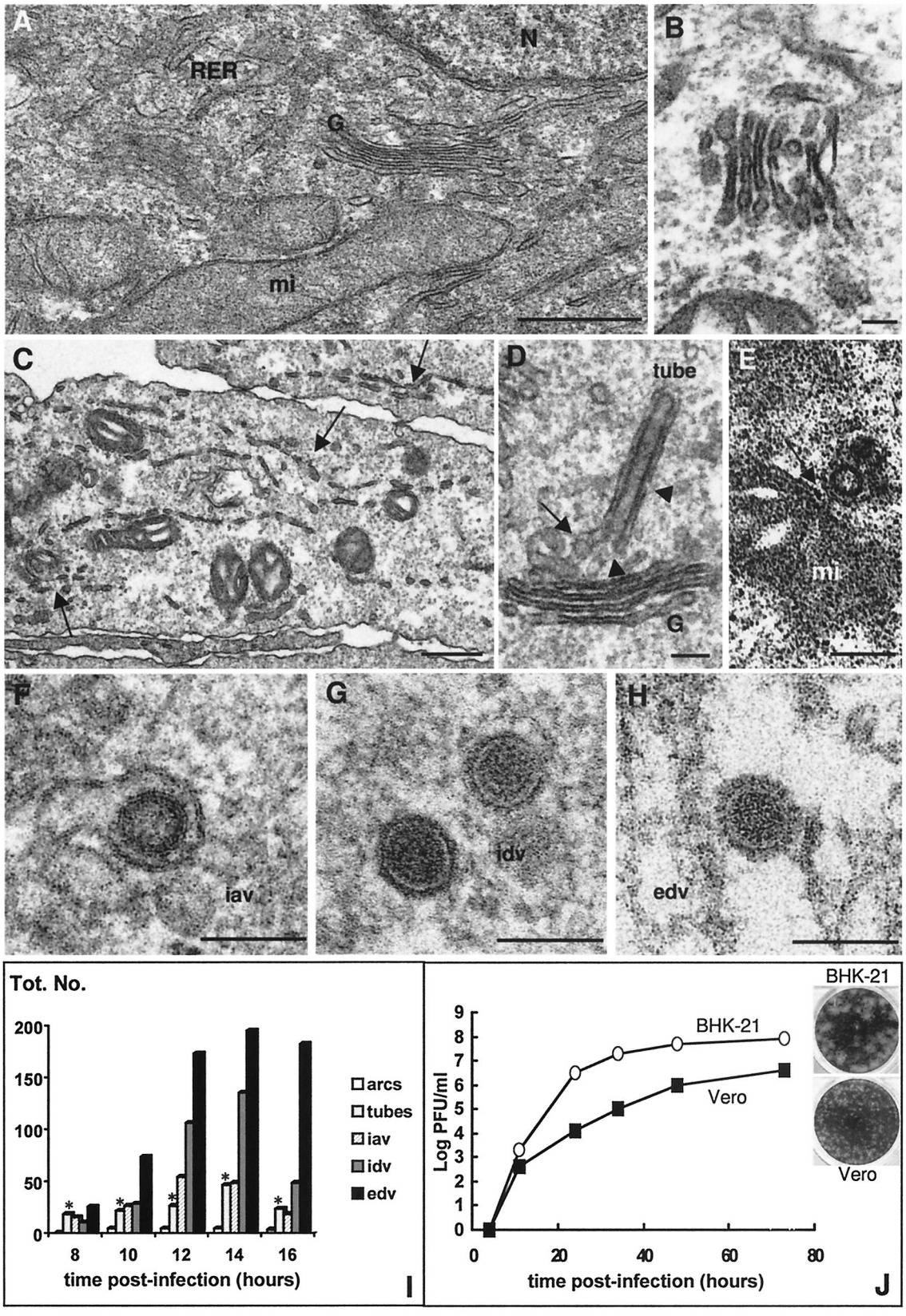

FIG. 6. Ultrastructural analysis of Bunyamwera virus infection in Vero cells. (A) Control, noninfected Vero cell with the characteristic organization of Golgi (G), RER, and mitochondria (mi). (B and C) Ultrastructure of infected Vero cells at 8 h p.i. A fragmented Golgi stack is shown in panel B, while general fragmentation of endomembranes is marked with arrows in panel C. (D to H) Bunyamwera virus-related

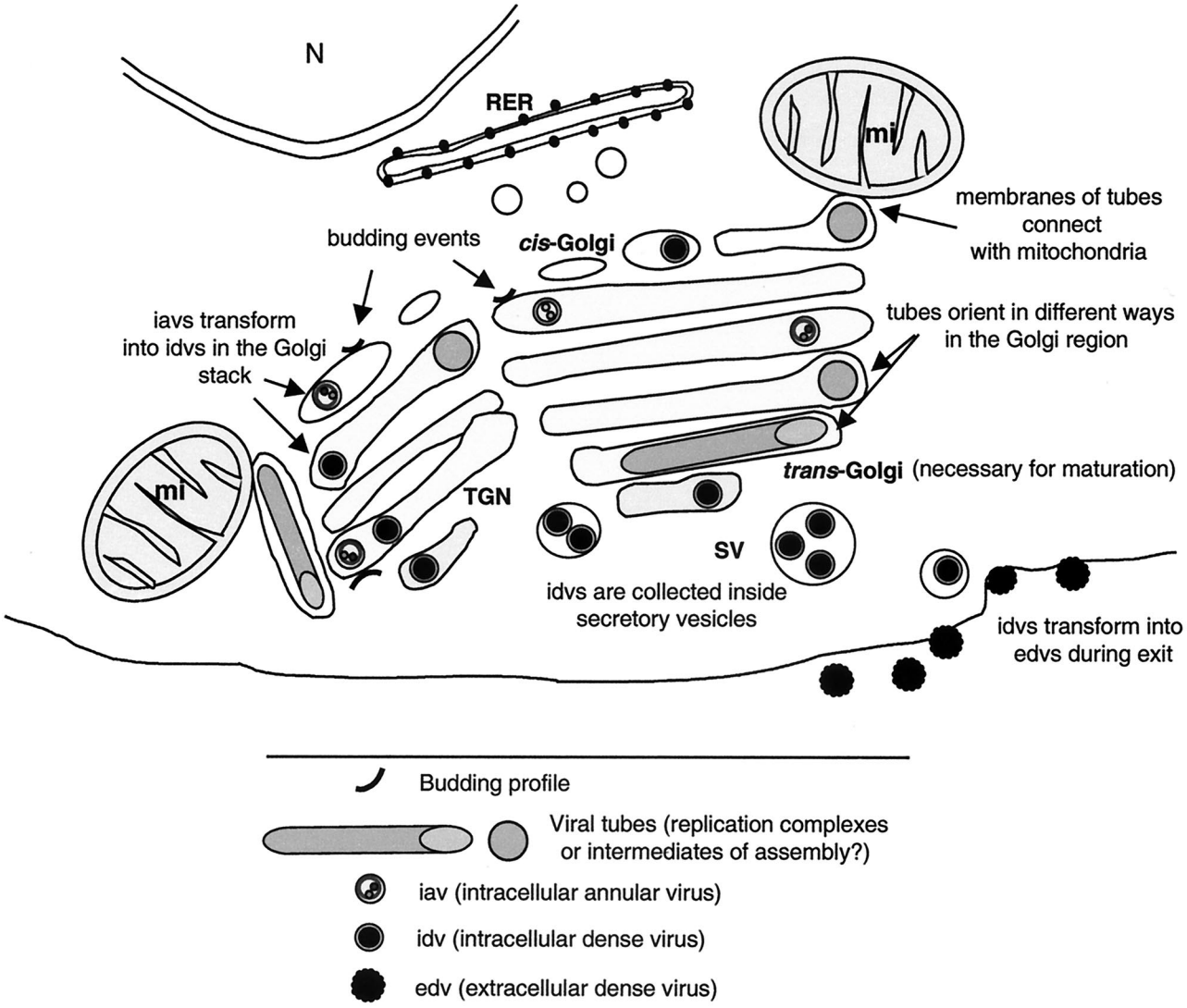

FIG. 7. Model for Bunyamwera virus assembly pathway showing the formation of the viral factory and the main maturation steps. Golgi stacks and mitochondria form a large complex, with viral tubes connecting them. Budding profiles, viral tubes, immature annular viruses, and mature dense viruses have been introduced in different locations within the Golgi stack, according to our experimental data.

bly and structural maturation take place in these complexes. Immature viruses transform into mature particles anywhere inside the stack while in the presence of a functional *trans*-Golgi, as demonstrated by using the *trans*-Golgi-disrupting drug MGM. Early in infection, tubes are seen in the Golgi region, where they often connect with surrounding mitochondria.

It is well known that different functions occur in different places within the Golgi stack. The *trans*-most Golgi cisternae and the *trans*-Golgi network have exclusive characteristics, such as a low pH and specific enzymes (glyco- and sulfotransferases, phosphatases, and endopeptidases) (8, 36). In particular, furin-type proteases (which are active at low pH) are involved in the proteolytic processing of some viral proteins during their transport through the Golgi (23). Structural transformation of bunyaviruses takes place at both the *cis* and *trans* sides of the Golgi in infected cells, but maturation cannot proceed without a functional *trans*-Golgi. This suggests that virions in the *cis*-Golgi could incorporate elements modified in the *trans* side and brought back to the *cis* side by retrograde

assemblies in Vero cells: tube in Golgi membranes showing connections with the Golgi stack (arrow) and areas open to the cytoplasm (arrowheads) (D); cross-sectioned tube attached to a mitochondrion (arrow) (E); iav in Golgi membranes (F); idv (G); and edv (H). Samples were processed by conventional processing in panels A to E, while freeze-substituted cells were used in panels F to H. (I) Quantification of the different viral assemblies found in Vero cells at different times p.i. Bars representing the amount of viral tubes are marked with asterisks. A total of 25 infected cells were studied at each time p.i., and 1,285 viral structures were included in the quantification. (J) Growth curves and plaque morphologies of Bunyamwera virus in BHK-21 and Vero cells. Bars, 0.5 μm (A); 1 μm (C); and 100 nm (B and D to H).

transport. Terminal glycosylation of viral proteins is a good candidate, although other modifications cannot be discounted. However, we cannot discount the possibility that maturation normally occurs in the *cis*-Golgi but is blocked when the *trans*-Golgi is perturbed due to the downstream effects of blocking membrane traffic. Whatever the mechanism operating for viruses inside the stack, some kind of a filter is established, since immature viral particles do not seem to exit the Golgi stack. For coronaviruses, immature particles are frequently seen in secretory vesicles and constitute about 1 to 5% of extracellular particles attached on the surface of infected cells (33). However, although thousands of viral particles have been analyzed in thin sections, we have not been able to detect immature bunyaviruses either inside secretory vesicles or on the cell surface.

The virus that exits the Golgi is not the same as that found in the extracellular environment: a second structural transformation takes place at the moment of secretion from the cell. This second maturation results in a prominent layer of round spikes. Although this second maturation step becomes evident as virions are released from cells, technical limitations meant that we cannot rule out the possibility that these changes occur intracelullarly. To characterize this step more adequately, cryomicroscopy and freeze-etching studies of purified intracellular viruses are now in progress.

Bunyamwera virus tubes. Our study has detected another new viral structure: tubular elements built in the Golgi region, which are surrounded by a membrane frequently connected with mitochondria. Although some of these tubes are inside Golgi sacculi, they are frequently located on the periphery of the Golgi stacks. Their membrane could then be derived from the endoplasmic reticulum as well. This could explain the potential continuities with mitochondria. Their role remains to be defined, but the fact that they are built early in infection, coincident with the EM detection of the first viral particles, and in rather fixed amounts (one to three per stack), suggests that they are not aberrant, late assemblies and points to a role in infection. Several options seem possible: they could be unusual replication complexes, even more unusual assembly intermediates, or structures for communication between the organelles building the "viral factory." There are no previous descriptions for morphogenetic intermediates or replication complexes with such a structure. However, we think that this latter option is possible, taking into account the observation that the number of tubes increases at the beginning of assembly and decreases when the release of viral particles reaches the highest levels. It is known that enveloped viruses that assemble intracellularly form their replication complexes in vesicles derived from intracellular membranes (18, 21, 35) while assembly can take place in a different location. If replication actually takes place in Golgi-associated viral tubes, the replicated genomes need to gain access to the cytoplasmic side of Golgi membranes for assembly. This could be taking place through open areas found in the tubes, where membranes are interrupted and are in communication with the cytoplasm. In situ colocalization of RNA synthesis and the viral polymerase will help us to understand if the viral tubes are indeed replication complexes or could play some other role during infection.

Another peculiar feature of the viral tubes is that they frequently connect with the external membrane of mitochondria recruited on the perinuclear area of the infected cell. Direct mitochondrion-Golgi contacts are also detected. Mitochondria are known to establish very close contacts with membranes belonging to the endoplasmic reticulum, through a mechanism regulated by calcium (38). However, the Golgi-mitochondrion associations we detected in both BHK-21 and Vero cells were induced by bunyavirus infection. Clustering of mitochondria on the perinuclear region of the cell has been detected in cells infected with rubella virus (4). In these cells, mitochondria are recruited around viral replication sites in modified endosomes and lysosomes, and this association has been proposed to provide the energy required for virus replication.

Assembly of Bunyamwera virus in Vero cells. Bunyamwera virus-infected Vero cells do not exhibit the typical pattern of a Golgi-associated virus as shown in infected BHK-21 cells. Rather, viral antigen is distributed as small dots all over the cytoplasm, and this is observed from the beginning of infection. This could indicate a different assembly pathway in Vero cells, since cell specific factors can be determinants of the morphogenesis and morphology of some viruses (32). However, visualization of the Golgi complex in infected Vero cells revealed a general fragmentation and dispersion of this compartment before accumulation of viral glycoproteins could be detected. Although the ERGIC and RER were also altered, no general cell lysis was observed. We first thought that disruption of cytoskeletal components could be involved in the early fragmentation of endomembranes in Vero cells. However, only microtubules showed some bundling, which was detected 2 h after fragmentation of membranes had been completed. Fragmentation and dispersal of the Golgi complex has also been observed during infection with herpes simplex virus in different cell types (7). This effect, mediated at least partly by fragmentation of microtubules, has been described as a late event caused by the huge influx of viral glycoproteins contained in virions and membranes flowing through the exocytic pathway. In bunyavirus-infected Vero cells, however, the effect is observed before the detection of viral glycoproteins or assembly of new viruses.

In spite of the significant structural alterations, in Vero cells the bunyavirus assembles in association with the remnants of Golgi stacks, where the first structural maturation also takes place. The same viral polymorphism (Golgi-associated tubes, iavs, idvs, and compact extracellular virions) was also observed in this cell type. Golgi-mitochondrion connections, sometimes mediated by viral tubes, were also seen. The early general fragmentation of endomembranes induced by the virus raises important questions, such as how assembly in the Golgi starts and how new viral particles are transported from the Golgi to the plasma membrane. Unconventional intracellular transport events could be involved.

In summary, a functional, although not necessarily structurally intact, Golgi complex is necessary for bunyavirus maturation in BHK-21 and Vero cells. Our future studies will focus on the identification of Golgi factors involved in the structural transformation of immature viruses inside the stack, the characterization of the second maturation step during transport of viruses from the Golgi to the extracellular environment, and the analysis of the potential function of viral tubes. These studies are now in progress.

ACKNOWLEDGMENTS

We express our gratitude to Balbino Alarcón for kindly providing the drug MGM and for helpful discussions. We also thank Manfred Renz and Hans P. Hauri for the anti-giantin antiserum and the monoclonal antibody against the ERGIC-53 protein, respectively, and José Ruiz Castón for critically reading the manuscript. Special thanks to Gloria Calderita and Sonia Ruiz for technical assistance with cell culture and cryoultramicrotomy, respectively.

I.J.S. and R.R.N. are recipients of fellowships for postgraduate students from the Gobierno Vasco and from the Ministerio de Ciencia y Tecnología of Spain, respectively. This work has been supported by grant BMC2000-0555 from the Ministerio de Ciencia y Tecnología (to C.R.), grant PB96-0818 from the Comisión Interministerial de Ciencia y Tecnología of Spain (to J.L.C.), and Wellcome Trust grant 048387 (to R.M.E.).

REFERENCES

1. **Anderson, G. W., and J. F. Smith.** 1987. Immunoelectron microscopy of Rift Valley Fever viral morphogenesis in rat primary hepatocytes. Virology **161:** 91–100.
2. **Andrés, G., R. García-Escudero, C. Simón-Mateo, and E. Viñuela.** 1998. African swine fever virus is enveloped by a two-membraned collapsed cisterna derived from the endoplasmic reticulum. J. Virol. **72:**8988–9001.
3. **Baker, T. S., N. H. Olson, and S. D. Fuller.** 1999. Adding the third dimension to virus life cycles: three-dimensional reconstruction of icosahedral viruses from cryoelectron micrographs. Microbiol. Mol. Biol. Rev. **63:**862–922.
4. **Beatch, M. D., and T. C. Hobman.** 2000. Rubella virus capsid associates with host cell protein p32 and localizes to mitochondria. J. Virol. **74:**5569–5576.
5. **Bonay, P., S. Munro, M. Fresno, and B. Alarcón.** 1996. Intra-Golgi transport inhibition by megalomicin. J. Biol. Chem. **271:**3719–3726.
6. **Bridgen, A., W. Friedemann, J. K. Fazakerley, and R. M. Elliott.** 2001. Bunyamwera bunyavirus nonstructural protein NSs is a nonessential gene product that contributes to viral pathogenesis. Proc. Natl. Acad. Sci. USA **98:**664–669.
7. **Campadelli, G., R. Brandimarti, C. Di Lazzaro, P. L. Ward, B. Roizman, and M. R. Torrisi.** 1993. Fragmentation and dispersal of Golgi proteins and redistribution of glycoproteins and glycolipids processed through the Golgi apparatus after infection with herpes simplex virus 1. Proc. Natl. Acad. Sci. USA **90:**2798–2802.
8. **Donaldson, J. G., and J. Lippincott-Schwartz.** 2000. Sorting and signaling at the Golgi complex. Cell **101:**693–696.
9. **Elliott, R. M.** 1997. Emerging viruses: the Bunyaviridae. Mol. Med. **3:**572–577.
10. **Goldsmith, C. S., L. H. Elliott, C. J. Peters, and S. R. Zaki.** 1995. Ultrastructural characteristics of Sin Nombre virus, causative agent of Hantavirus pulmonary syndrome. Arch. Virol. **140:**2107–2122.
11. **Griffiths, G., and P. Rottier.** 1992. Cell biology of viruses that assemble along the biosynthetic pathway. Semin. Cell Biol. **3:**367–381.
12. **Hobman, T. C., L. Woodward, and M. G. Farquhar.** 1992. The rubella virus E1 glycoprotein is arrested in a novel post-ER, pre-Golgi compartment. J. Cell Biol. **118:**795–811.
13. **Huovila, A. J., A. M. Eder, and S. D. Fuller.** 1992. Hepatitis B surface antigen assembles in a post-ER, pre-Golgi compartment. J. Cell Biol. **118:**1305–1320.
14. **Jäntti, J., P. Hildén, H. Rönkä, V. Mäkiranta, S. Keränen, and E. Kuismanen.** 1997. Immunocytochemical analysis of Uukuniemi virus budding compartments: role of the intermediate compartment and the Golgi stack in virus maturation. J. Virol. **71:**1162–1172.
15. **Kellenberger, E.** 1991. The potential of cryofixation and freeze-substitution: observations and theoretical considerations. J. Microsc. **161:**183–203.
16. **Krijnse-Locker, J., M. Ericsson, P. J. Rottier, and G. Griffiths.** 1994. Characterization of the budding compartment of mouse hepatitis virus: evidence that transport from the RER to the Golgi complex requires only one vesicular transport step. J. Cell Biol. **124:**55–70.
17. **Lappin, D. F., G. W. Nakitare, J. W. Palfreyman, and R. M. Elliott.** 1994. Localization of Bunyamwera bunyavirus G1 glycoprotein to the Golgi requires association with G2 but not with NSm. J. Gen. Virol. **75:**3441–3451.
18. **Magliano, D., J. A. Marshall, D. S. Bowden, N. Vardaxis, J. Meanger, and J.-Y. Lee.** 1998. Rubella virus replication complexes are virus-modified lysosomes. Virology **240:**57–63.
19. **Matsuoka, Y., S. Y. Chen, and R. W. Compans.** 1994. A signal for Golgi retention in the bunyavirus G1 glycoprotein. J. Biol. Chem. **269:**22565–22573.
20. **McIntosh, J. R.** 2001. Electron microscopy of cells: a new begining for a new century. J. Cell Biol. **153:**F25–F38.
21. **Mckenzie, J. M., M. K. Jones, and E. G. Westway.** 1999. Markers for *trans*-Golgi membranes and the intermediate compartment localize to induced membranes with distinct replication functions in flavivirus-infected cells. J. Virol. **73:**9555–9567.
22. **Mettenleiter, T. C.** 2002. Herpervirus assembly and egress. J. Virol. **76:**1537–1547.
23. **Moehring, J. M., N. M. Inocencio, B. J. Robertson, and T. J. Moehring.** 1993. Expression of mouse furin in a Chinese hamster cell resistant to *Pseudomonas* exotoxin A and viruses complements the genetic lesion. J. Biol. Chem. **268:**2590–2594.
24. **Moss, B.** 1996. *Poxviridae:* the viruses and their replication, p. 2637–2761. *In* B. N. Fields, D. M. Knipe, and P. M. Howley (ed.), Fields virology, 3rd ed. Lippincott-Raven, Philadelphia, Pa.
25. **Murphy, F. A., A. K. Harrison, and S. G. Whitfield.** 1973. Morphologic and morphogenetic similarities of Bunyamwera serological supergroup viruses and several other arthropod-borne viruses. Intervirology **1:**297–316.
26. **Nakitare, G. W., and R. M. Elliott.** 1993. Expression of the Bunyamwera virus M genome segment and intracellular localization of NSm. Virology **195:**511–520.
27. **Risco, C., and J. L. Carrascosa.** 1999. Visualization of viral assembly in the infected cell. Histol. Histopathol. **14:**905–926.
28. **Risco, C., L. Menéndez-Arias, T. D. Copeland, P. Pinto da Silva, and S. Oroszlan.** 1995. Intracellular transport of murine leukemia virus during acute infeçtion of NIH 3T3 cells: nuclear import of nucleocapsid protein and integrase. J. Cell Sci. **108:**3039–3050.
29. **Risco, C., M. Muntión, L. Enjuanes, and J. L. Carrascosa.** 1998. Two types of virus-related particles are found during transmissible gastroenteritis virus morphogenesis. J. Virol. **72:**4022–4031.
30. **Risco, C., and P. Pinto da Silva.** 1998. The fracture-flip technique reveals new structural features of the *Escherichia coli* cell wall. J. Microsc. **189:**213–218.
31. **Risco, C., J. R. Rodríguez, C. López-Iglesias, J. L. Carrascosa, M. Esteban, and D. Rodríguez.** 2002. Endoplasmic reticulum-Golgi intermediate compartment membranes and vimentin filaments participate in vaccinia virus assembly. J. Virol. **76:**1839–1855.
32. **Roberts, P. C., and R. W. Compans.** 1998. Host cell dependence of viral morphology. Proc. Natl. Acad. Sci. USA **95:**5746–5751.
33. **Salanueva, I. J., J. L. Carrascosa, and C. Risco.** 1999. Structural maturation of the transmissible gastroenteritis coronavirus. J. Virol. **73:**7952–7964.
34. **Schmaljohn, C. S., and J. W. Hooper.** 2001. *Bunyaviridae:* the viruses and their replication, p. 1581–1602. *In.* D. M. Knipe, P. M. Howley, and D. E. Griffin (ed.), Fields virology. Lippincott Williams & Wilkins, Philadelphia, Pa.
35. **Snijder, E. J., H. van Tol, N. Roos, and K. W. Pedersen.** 2001. Non-structural proteins 2 and 3 interact to modify host cell membranes during the formation of the arterivirus replication complex. J. Gen. Virol. **82:**985–994.
36. **Sossin, W. S., J. M. Fisher, and R. H. Scheller.** 1990. Sorting within the regulated secretory pathway occurs in the trans-Golgi network. J. Cell Biol. **110:**1–12.
37. **Visa, N., A. T. Alzhanova-Ericsson, X. Sun, E. Kiseleva, B. Bjorkroth, T. Wurtz, and B. Daneholt.** 1996. A pre-mRNA-binding protein accompanies the RNA from the gene through the nuclear pores and into polysomes. Cell **84:**253–264.
38. **Wang, H. J., G. Guay, L. Pogan, R. Sauvé, and I. R. Nabl.** 2000. Calcium regulates the association between mitochondria and a smooth subdomain of the endoplasmic reticulum. J. Cell Biol. **150:**1489–1497.
39. **Watret, G. E., G. R. Pringle, and R. M. Elliott.** 1985. Synthesis of Bunyavirus-specific proteins in a continuous cell line (XTC-2) derived from *Xenopus laevis.* J. Gen. Virol. **66:**473–482.
40. **Weber, F., E. F. Dunn, A. Bridgen, and R. M. Elliott.** 2001. The Bunyamwera virus nonstructural protein NSs inhibits viral RNA polymerase in a minireplicon system. Virology **281:**67–74.